**BIBECHANA**
Vol. 21, No. 3, December 2024, 213-220

ISSN 2091-0762 (Print), 2382-5340 (Online)
Journal homepage: http://nepjol.info/index.php/BIBECHANA
Publisher: Dept. of Phys., Mahendra Morang A. M. Campus (Tribhuvan University) Biratnagar

# Photoluminescence properties of $Tm^{3+}/Ho^{3+}/Cr^{3+}$-co-doped $Y_3AlGa_4O_{12}$ nano-garnet phosphors for visible-NIR LED applications

**Ramadevi Nepal[1], Jyothi Prasad G.M.[2,3], Praveena Ravipati[3,*], B.D. Joshi[4,**], D. Sujatha[5]**

[1]*Central Department of Physics, Tribhuvan University, Kirtipur, Kathmandu, Nepal.*
[2]*Andhra University, Visakhapatnam -530003, India.*
[3]*Department of Physics, Gayatri Vidya Parishad College of Engineering (A), Visakhapatnam- 530048, India.*
[4]*Department of Physics, Siddhanath Science Campus, Tribhuvan University, Mahendranagar, Nepal.*
[5]*GVSM Govt. Degree College, Ulavapadu, SPSR Nellore – 523292, India.*

[*]Corresponding author: Email: praveena@gvpce.ac.in
[**]Corresponding author: Email:bhawani.joshi@snsc.tu.edu.np

**Abstract**

*Trivalent lanthanide ($Ln^{3+}$; Ln = Tm, Ho, Cr)-doped $Y_3AlGa_4O_{12}$ nano-garnet phosphor powders with varying $Cr^{3+}$ ion concentration (0.5, 1.0, 2.0 and 3.0 mol%) were prepared using sol-gel synthesis. The prepared powders were characterized by X-ray powder diffraction (XRD), Raman and photoluminescence spectroscopic techniques. Phase purity, structure and crystallite size have been estimated from the XRD results. Raman spectra showed the vibrational analysis of the prepared powders. Excitation spectrum showed a broad band centred at 354 nm when monitored at 712 nm. Under 360 nm excitation, emission spectra showed a broad band with characteristic peaks of $Tm^{3+}$, $Ho^{3+}$ and $Cr^{3+}$ ions. The intensity of peaks and full width at half maximum were increased up to 2.0 mol% $Cr^{3+}$ ion and then decreased. All the decay curves exhibited non-exponential nature with an average lifetime of 0.302 ms. The decay curves were found to be insensitive to the $Cr^{3+}$ ion concentration. The CIE colour co-ordinates were located in the orange-red region of the CIE diagram with correlated colour temperature 2261 K. The results showed that the present phosphors were suitable for the solid state light emitting diode applications.*

**Keywords**
Tm, Ho, Cr, YAGG, garnets, phosphors, light emitting diode

**Article information**
Manuscript received: February 19, 2024; Revised: April 23, 2024; Accepted: April 26, 2024
DOI https://doi.org/10.3126/bibechana.v21i3.62845

## 1 Introduction

Nanomaterials like nanowires or nano-phosphors can improve electron and photon management within the light emitting diodes (LEDs) structure, leading to reduced energy consumption and increased luminous efficiency. Nanoparticles provide a high level of tunability, allowing for the customization of various properties such as colour, conductivity, and thermal management. This flexibility enables the tailoring of LED materials to meet specific application requirements, leading to advancements in diverse fields, including lighting, displays, and optoelectronics. Nanoparticles enable the miniaturization of LED components, allowing for the creation of smaller, more compact devices. This is particularly important in the development of flexible and bendable LED displays, where the use of nanomaterials helps to maintain the required structural integrity while achieving the desired flexibility.

Recently, research on nano-phosphors has received significant attention as these are efficient luminescent materials for LEDs, field emission displays and plasma displays. Phosphor-converted LEDs has excellent properties such as less production cost and simple device structure [1]. Further, near infrared (NIR) broadband sources are very important for non-invasive medical diagnostics, non-destructive food measurement, bioimaging, night-vision technologies, light converters and optical amplifiers [2–6]. The conventional incandescent bulbs and halogen lamps face different problems like low efficiency, short lifetime, high working temperatures and large size which limit their applications [7]. On the other hand, NIR-emitting LEDs have great advantages like high efficiency, long lifetime, small in size, etc. Therefore, NIR broad band sources with these features are highly desired in wide range of applications [8].

NIR phosphor-converted LEDs contains a InGaN blue LED chip with NIR-emitting phosphors which can bring together the great advantages of InGaN LED chips including higher thermal stability, low manufacturing cost and high luminous efficiency [9] [10]. Besides, broadband and light converters can be realized by the careful selection of host material and emitting ion of NIR phosphors [11]. Trivalent lanthanide ($Ln^{3+}$) ions have been extensively employed as emitting ions for various phosphor-converted LEDs. Among the various $Ln^{3+}$ ions, $Tm^{3+}$ is one of the most interesting ions as it provides blue and red emissions whereas $Ho^{3+}$ ion is famous for its green emission. Therefore, many researchers have focused on the development of single phased phosphors co-doped with both $Tm^{3+}$ and $Ho^{3+}$ ions and studied the energy transfer between $Tm^{3+}$ and $Ho^{3+}$ ions excited by NIR wavelength [12, 13]. In our previous work, ultraviolet excited (UV) $Tm^{3+}$ and $Ho^{3+}$ co-doped $Y_3Al_4GaO_{12}$ phosphors were prepared and studied their luminescence and energy transfer properties for white LED applications [14]. In the present work, $Tm^{3+}/Ho^{3+}$:$Y_3AlGa_4O_{12}$ (YAGG) phosphors co-doped with $Cr^{3+}$ ions were prepared in order to broaden and extend the spectral profile in to the NIR region for broadband source applications. $Cr^{3+}$ ion is the interesting ion to dope into the inorganic materials owing to its deep red colours (~ 700 nm) and narrow band emissions due to the spin-forbidden $^2E \rightarrow {}^4A_2$ transition or broadband emission (650-1600 nm) due to the spin-allowed $^4T_2 \rightarrow {}^4A_2$ transition, which strongly depends on the surrounding crystal-field strength given by the host lattices [15–17].

Garnets have been chosen as the host materials for this purpose owing to their excellent properties like high thermal conductivity, high chemical stability and exhibit intense luminescence when doped with $Ln^{3+}$ ions [18]. $Ln^{3+}$:$Y_3Al_5O_{12}$ (YAG) is the well-known commercial phosphor for LED applications [19] . However, the search for the advanced phosphors with better multiple properties for display applications is still remaining as challenging task. In this regard, the chemical composition of the garnets can be changed by replacing the part of the $Al^{3+}$ ions with the $Ga^{3+}$ or $Fe^{3+}$ or $Ge^{3+}$ ions and/or $Y^{3+}$ ions with $Lu^{3+}$ or $Gd^{3+}$ ions. When the $Al^{3+}$ ions are replaced by larger $Ga^{3+}$ ions, the distance between dodecahedral lattice sites (where the $Ln^{3+}$ ion is substituted) is going to be increased. This increase in the distance between the $Ln^{3+}$ ions tends to decrease the interaction between them in the host matrix and in turn reduces the concentration quenching [20]. This would enhance the luminescence intensity and efficiency as well. For instance, it was predicted theoretically that the $Ga^{3+}$ garnets show better luminescence properties when compared to $Al^{3+}$ garnets [21]. The same was also observed by Praveena et al., [22] where the luminescence intensity of $Dy^{3+}$-doped $Y_3AlGa_4O_{12}$ nano-garnets are higher than that of $Y_3Al_4GaO_{12}$ nano-garnets. Hence, the authors are motivated to investigate the luminescence properties of the present $Tm^{3+}/Ho^{3+}/Cr^{3+}$:YAGG phosphors by varying the $Cr^{3+}$ ion concentration. To the best of author's knowledge, no report is found on the current study.

## 2 Experimental technique

In the present study the phosphors were synthesised by the well-know sol-gel method [23]. Sol-gel synthesis is a versatile method for producing phosphors with tunable properties, including structural and optical characteristics. Optimizing synthesis

parameters can significantly impact the final product's properties. For instance, the choice of precursors can affect the chemical composition, dopant concentration and crystal structure of the phosphor which can influence the luminescence properties. The solvent affects the solubility of precursors and the rate of hydrolysis and condensation reactions. It can also impact the porosity, homogeneity and surface area of the phosphor. The pH of the so-gel solution can influence the hydrolysis and condensation reactions, affecting the size, morphology, and crystallinity of the phosphor particles. pH adjustment can also help control the distribution of dopants in the host matrix. The temperature and duration of the sol-gel process can affect the kinetics of the reaction, influencing the phase composition, crystallinity, and particle size of the phosphor. Higher temperatures and longer reaction times generally lead to larger, more crystalline particles. The drying and calcinations processes can impact the phase purity, crystallinity, and luminescence properties of the phosphor. Controlled drying and calcinations can help prevent phase transformations and enhance the phosphor's optical properties. The concentration of dopants in the sol-gel solution can affect the luminescence efficiency and colour of the phosphor. Optimizing the dopant concentration is crucial for achieving the desired optical properties. The addition of additives and surfactants can influence the morphology, particle size, and dispersion of the phosphor. This can also affect the luminescence efficiency and stability of the phosphor. Post-treatment processes, such as annealing or surface modification, can further enhance the structural and optical properties of the phosphor. These processes can help to improve the crystallinity, phase purity, and luminescence efficiency of the phosphor. Therefore, optimizing sol-gel synthesis parameters is essential for tailoring the structural and optical properties of phosphors. Considering aforementioned parameters, the following optimizing conditions were taken into consideration after performing several experiments.

YAGG nano-crystalline powders tri-doped with dopant concentrations of 0.1 $Tm^{3+}$/0.3 $Ho^{3+}$/x $Cr^{3+}$ ions (where x= 0.5, 1.0, 2.0, 3.0 mol%) were prepared [23]. Nitrate forms of the precursors were dissolved into the 25 ml of 1M $HNO_3$ under stirring to get 'sol'. pH is maintained at around 1. Citric acid and PEG were added to the solution in the ratio metal:citric acid:PEG is 1:2:8. Continued stirring for 2 h till the 'gel' is obtained and then heated at 90 °C for 40 h. No other additives and surfactants were used. Then, the obtained yellow colour gel was first heated at 500 °C for 4 h and later at 950 °C for 16 h in an electronic furnace with air atmosphere. The final product is in the white colour nano-crystalline powder form.

XRD patterns were recorded using X-ray diffractometer (Philips PW 1830) using Cu K radiation (1.5406 Å). Confocal micro-Raman spectrometer (Horiba Jobin Yvon Lab RAM-HR 800) was used to record the Raman spectrum. Excitation, emission and decay spectra were recorded by using JOBIN YVON Flurolog – 3 spectrofluorimeter with a 450 W xenon flash lamp. All the measurements were carried out at the similar conditions.

## 3 Results and Discussion

### 3.1 X-ray diffraction

XRD profiles of the tri-doped YAGG garnet nano-crystalline powders are displayed in the Fig. 1. All the diffraction peaks were well matched with the standard JCPDS data card no. 89-6661 that corresponds to space group of Ia-3d cubic structure. No impurity peak is identified. This indicates that the formation of single phase high purity phosphors and successful incorporation of dopant ions without causing any disruptions in the crystal structure of YAGG. The well resolved sharp peaks suggest that the synthesized samples are highly crystalline in nature. From Fig. 1, it is clear that the crystallinity is increased with increasing $Cr^{3+}$ ion concentration. The crystallite size of the powder samples was estimated using Debye-Scherrer's equation $D_{hkl} = k\lambda/\beta\cos\vartheta$, where D is the average crystallite size, k is the shape factor (0.9), is the wavelength of the X-rays, is the full width at half maximum (FWHM) and is the diffraction angle. The crystallite size is increased from 13.8 to 23.7 nm when the $Cr^{3+}$ concentration is increased from 0.5 to 3 mol%. The crystallite size was slightly reduced upon adding the $Cr^{3+}$ into the Tm,Ho-doped YAGG host [14] which represents the enhanced surface area.

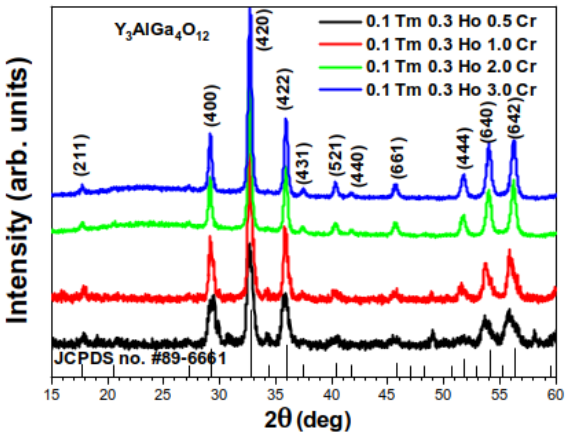


Figure 1: XRD profiles of the tri-doped YAGG nano-crystalline powders.

### 3.2 Raman spectra

The Raman spectrum of 1.0 mol% $Cr^{3+}$ tri-doped YAGG samples is shown in Fig. 2. The high frequency modes (800–1000 $cm^{-1}$) are associated to symmetric and asymmetric internal stretching vibrations of rigid $AlO_4/GaO_4$ tetrahedra and the modes lying between 450–800 $cm^{-1}$ are assigned to bending motions of these tetrahedra. The remaining lattice modes (150– 450$cm^{-1}$) involve rotations and translations of the $AlO_4/GaO_4$ groups, octahedrally co-ordinated trivalent cations and dodecahedrally co-ordinated trivalent cations [22, 24, 25].

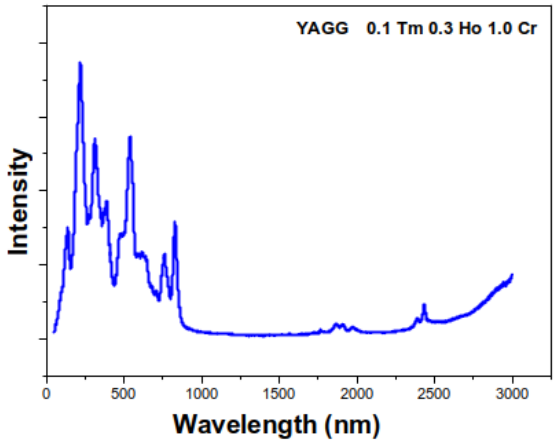


Figure 2: Raman spectrum of tri-doped YAGG nano-crystalline powder.

### 3.3 Excitation

It is well-known that $Cr^{3+}$ has $^2E$, $^4A_2$, $^4T_2$ and $^4T_1$ energy levels come from the 4F term in its $d^3$ configuration [26, 27]. The excitation and luminescence properties of the $Cr^{3+}$ ion depend on the relative positions of the $^4T_2$ and $^2E$ levels. $^4T_2$ state is above the $^2E$ level when the $Cr^{3+}$ ion locates in the intermediate-field site that results R-line emission whereas $^4T_2$ is under the $^2E$ level when the $Cr^{3+}$ ion locates in the weak-field site. Figure 3 shows the excitation spectrum of 1 mol% $Cr^{3+}$ tri-doped YAGG sample monitoring at emission wavelength of 712 nm. The spectrum consists of broadband in the region 300-450 nm which corresponds to $^4A_2 \rightarrow {}^4T_1$ ($^4F$) transition of $Cr^{3+}$ ion [28]. From Fig. 3 it is confirmed that the present samples can be excited by near UV and visible radiation that is matching with InGaN LED chip.

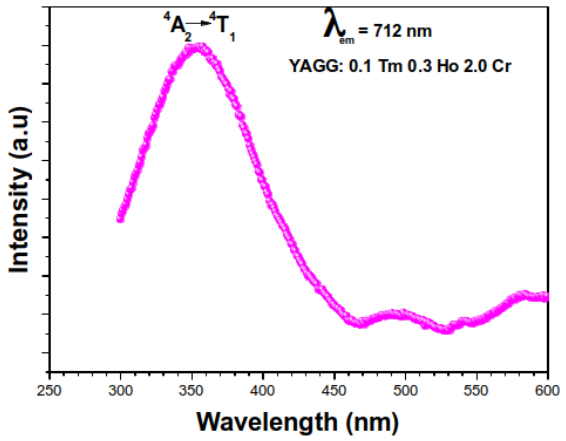


Figure 3: Excitation spectra of tri-doped YAGG sample.

### 3.4 Photoluminescence

Figure 4 shows the photoluminescence spectra of tri-doped YAGG nano-crystalline powders excited with the wavelength of 360 nm. The spectra have a broad band in the region 450-800 nm with sharp characteristic peaks. The peaks are located at 482, 523, 557, 582, 612, 640 and 712 nm. The peak at 482 nm corresponds to $^1G_4 \rightarrow {}^3H_6$ transition of $Tm^{3+}$ ion, peaks at 523 and 557 nm correspond to $^5F_4$, $^5S_2 \rightarrow {}^5I_8$ transitions of $Ho^{3+}$ ion, peaks at 582 and 612 nm correspond to $^4T_2 \rightarrow {}^4A_2$ transition of $Cr^{3+}$ ion, peak at 640 nm correspond to $^1G_4 \rightarrow {}^3F_4$ transition of $Tm^{3+}$ ion and peak at 712 nm correspond to $^2E \rightarrow {}^4A_2$ transition of $Cr^{3+}$ ion [14, 28, 30]. Rai et. al., [31] also noticed the 581 and 700 nm emissions of $Cr^{3+}$ in $LaVO_4$ host upon excited with wavelengths of 428 and 467 nm. Yao et. al., [32] also observed the similar type of sharp lines at higher wavelengths side of the $^2E \rightarrow {}^4A_2$ transition corresponding to $Nd^{3+}$ ion when it is co-doped with $Cr^{3+}$ ion into the $Ca_3Sc_2SiO_{12}$ host. Chen et. al., [33] reported the $Yb^{3+}/Ln^{3+}/Cr^{3+}$ (Ln = Er, Ho) doped transparent glass ceramics: crystallization, $Ln^{3+}$ sensitized $Cr^{3+}$ upconversion emission and multimodal temperature sensing. An intense $Cr^{3+}$ upconversion luminescence assigned to the $^2E \rightarrow {}^4A_2$ transition was observed upon 980 nm laser excitation via energy transfer from $Yb^{3+}$ sensitizers to $Er^{3+}$ activators/bridging-centers and finally to $Cr^{3+}$ emitting centers. Zhang et. al., [34] observed the enhanced photoluminescence of $Gd_3Al_4GaO_{12}$ (GAGG):$Cr^{3+}$ by energy transfer from co-doped $Dy^{3+}$ ions. From Fig. 4, it is observed that the luminescence intensity is slightly increased up to 2 mol% of $Cr^{3+}$ and then decreased which represents the optimum concentration is 2.0 mol%. From Fig. 4, it is noticed that the intensity variation with respect to $Cr^{3+}$ ion is very less and hence these

are stable phosphors. The FWHM values of the emission band are found to be 75.3, 77.3, 88.1 and 81.2 nm for 0.5, 1.0, 2.0 and 3.0 mol% of $Cr^{3+}$ ion, respectively. These values are also slightly increased up to 2.0 mol% and then decreased. Hence, the optimised concentration is 2.0 mol%. Further, it is observed that the FWHM is higher than that of YAGG:0.5Tm,1.5Ho host (~65 nm) [14] and $MgAlGa_{0.7}B_{0.3}O_4:Cr^{3+}$(29 nm) at lower concentrations [35]. Thus, with the addition of $Cr^{3+}$ ion to the YAGG:Tm/Ho host increased the FWHM value. Therefore, from the luminescence spectra it is concluded that these phosphor powders can be useful for the broadband visible-NIR light emitting diode applications.

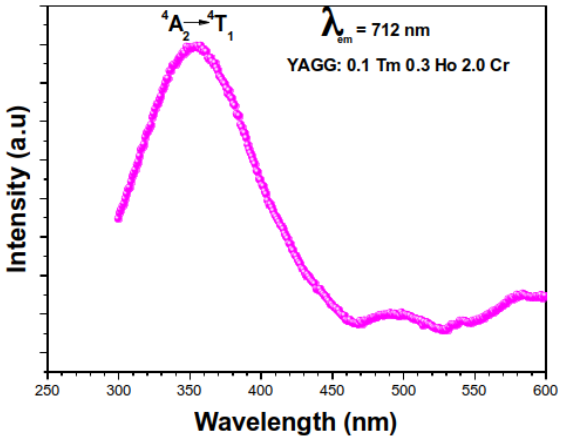


Figure 4: The photoluminescence spectra of tri-doped YAGG nano-crystalline powders.

### 3.5 Decay spectra

Figure 5 shows the decay curves monitoring at 582 nm emission and excited by 360 nm wavelength. All the decay curves exhibit non-exponential nature but insensitive to the $Cr^{3+}$ ion concentration. The non-exponential nature indicates the energy transfer processes are involved among $Tm^{3+}$, $Ho^{3+}$ and $Cr^{3+}$ ions. The insensitive nature of decay curves over $Cr^{3+}$ ion concentration represents the absence of concentration quenching in these phosphors, which enhances the luminescence efficiency. The average lifetime is found to be around 0.302 ms which is comparable with that of $Cr^{3+}$:$LaVO_4$ host (0.4503 ms) [31], higher than that of $Cr^{3+}$-doped garnets like YGG (0.240 ms), GGG (0.160 ms), YSGG (0.140 ms), GSAG (0.150 ms) and GSGG (0.120 ms) [36] and $Cr^{3+}$:$LuScO_3$ (0.023 ms) hosts [37].

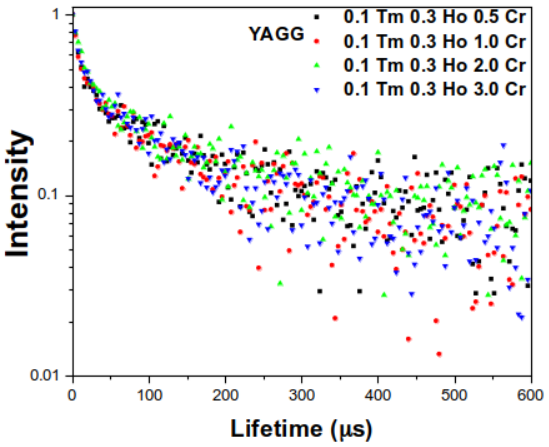


Figure 5: The decay profiles of tri-doped YAGG phosphors excited at 360 nm wavelength.

### 3.6 Energy transfer among $Tm^{3+}$,$Ho^{3+}$ and $Cr^{3+}$

The energy transfer among $Tm^{3+}$, $Ho^{3+}$ and $Cr^{3+}$ ions in the YAGG host can be elucidated through the schematic energy level diagram depicted in Fig. 6. When subjected to 360 nm excitation, first the $Tm^{3+}$ ions get excited from $^3H_6$ to the $^1D_2$ level. Subsequently, these ions undergo non-radiative relaxation (NR) to the lower $^1G_4$ level. Following this relaxation, radiative decay of $Tm^{3+}$ ions to the ground state takes place, emitting photons at wavelengths 482 nm and 640 nm, corresponding to the $^1G_4 \rightarrow {}^3H_6$ and $^1G_4 \rightarrow {}^3F_4$ transitions, respectively. During this process, a fraction of the energy is transferred from the excited $Tm^{3+}$ ions to adjacent ground state $Ho^{3+}$ ions through energy transfer (ET1): $^1D_2(Tm) + {}^5I_8(Ho) \rightarrow {}^3F_4(Tm) + {}^5G_6(Ho)$. This phenomenon arises due to pronounced spectral overlap between the $Tm^{3+}$ emission ($^1D_2 \rightarrow {}^3F_4$) and $Ho^{3+}$ excitation ($^5I_8 \rightarrow {}^5G_6$) in the vicinity of 460 nm [14]. Subsequently, the excited $Ho^{3+}$ ions undergo non-radiative relaxation to lower levels, followed by radiative transitions, $^5F_4 \rightarrow {}^5I_8$ (523 nm) and $^5S_2 \rightarrow {}^5I_8$ (557 nm). Concurrently, $Cr^{3+}$ ions are also elevated to the $^4T_1$ level from $^4A_2$ upon 360 nm excitation. These ions undergo non-radiative transitions to lower levels, populating the $^2E$ and $^4T_2$ levels. Notably, a strong yellow emission at 582 nm and a relatively weak red emission at 612 nm are observed from the $Cr^{3+}$ energy levels, corresponding to the $^4T_2 \rightarrow {}^4A_2$ transition, along with NIR emission at 712 nm associated with the $^2E \rightarrow {}^4A_2$ transition of $Cr^{3+}$ ions. In addition to this, $Cr^{3+}$ ions transfer a portion of their energy to adjacent $Ho^{3+}$ ions (ET2), populating the $^5F_4$ and $^5S_2$ excited levels of $Ho^{3+}$. This energy transfer is reflected in the emission spectra (Fig. 4), where the intensity at 523 nm and 577 nm increases with increase in $Cr^{3+}$ ion

concentration up to 2.0 mol% and then decreases.

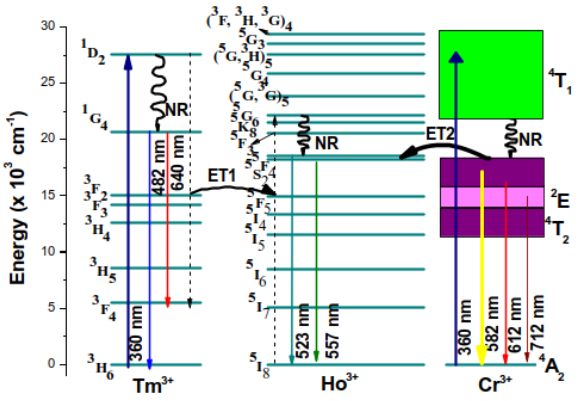


Figure 6: Schematic partial energy level diagram of YAGG:Tm,Ho,Cr nano-phosphors. Solid lines with arrow represent the transitions between the energy levels, zigzag lines indicate non-raditative transitions (NR), and ET represents energy transfer.

### 3.7 CIE colour co-ordinates

Commission International de I'Eclairage (CIE) colour co-ordinates and chromaticity diagrams provide a globally recognized and standardized system for describing colours accurately [38]. This consistency is vital for industries to ensure colour fidelity across various materials. These co-ordinates and diagrams are used to study colour perception, human vision and lighting technologies. Figure 7(a) display the CIE chromaticity diagram and 7(b) represent the corresponding spectral profile of the 2.0 mol% $Cr^{3+}$ tri-doped YAGG phosphor. The colour co-ordinates (x, y = 0.5304, 0.4611) are located in the orange-red region with correlated colour temperature 2261 K. This represents the present phosphor gives a warm light [39]. The colour co-ordinates in the present host are closer to the YAGG:0.5Tm,1.5Ho [14], as the ratio of Tm/Ho concentration is same, but shifted towards orange-red side with the addition of $Cr^{3+}$ ion. An LED device fabricated with the GAGG:0.1$Cr^{3+}$,0.01$Dy^{3+}$ phosphor and a 450 nm blue chip showed the CIE coordinates at (0.6387, 0.2873) [34]. It appears as a milky white light in the LED device and provides a bright purplish-red emission driven by a current of 20 mA. It gives a strong red emission and yields a luminous efficacy of 27.8 $lmW^{-1}$. In addition, chlorophyll pigment in plants absorbs blue (400-500 nm) and red (600-700 nm) light to help photosynthetic and phototropic processes [40]. Phytochrome in plants changes its state to active form in the red light (600-700 nm, peaking at 660 nm) and inactive form in the far-red light (600-780 nm, peaking at 730 nm) [41]. These two pigments respond to red light in particular to support several functionalities in plants. Therefore, the Tm/Ho/Cr-doped YAGG nano-crystalline powders can also be used in the plant growth LED applications.

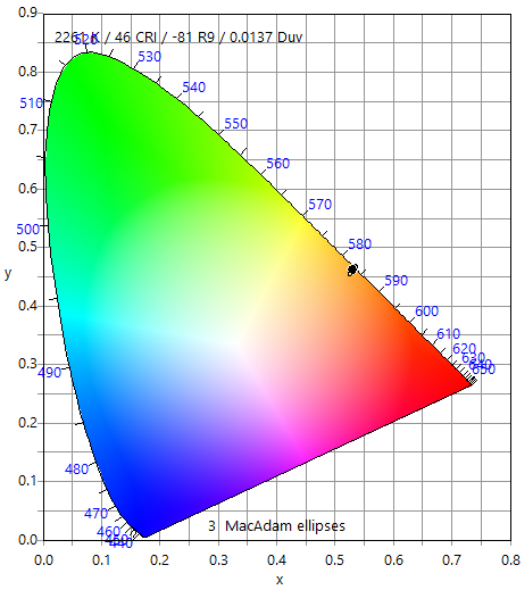


(a)

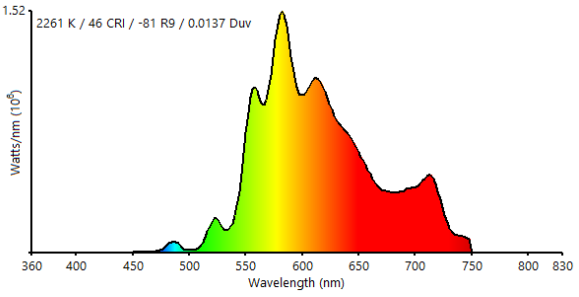


(b)

Figure 7: (a) CIE diagram (b) corresponding spectral profile of 2.0 mol% $Cr^{3+}$ samples.

## 4 Conclusions

$Tm^{3+}$/$Ho^{3+}$/$Cr^{3+}$ tri-doped YAGG nano-crystalline powders were prepared by sol-gel method and are characterized by XRD, Raman and photoluminescence measurements. The XRD results confirmed the formation of single phased cubic garnet structure. The Raman spectrum provided the vibrational analysis of the present samples. Excitation spectrum showed that these phosphors can be successfully excited with near UV LED light. The photoluminescence spectra showed the broad band in the visible and NIR regions with characteristic peaks of $Tm^{3+}$/$Ho^{3+}$/$Cr^{3+}$ions. The addition of $Cr^{3+}$ ion increased the FWHM value. The decay curves were invariant with the $Cr^{3+}$ ion

concentration which indicates that the absence of concentration quenching. The CIE co-ordinates fell in the orange-red region. The results showed that the present phosphors have potential applications in the visible-NIR light emitting broadband sources and plant growth LED technology.

**Acknowledgements**

The authors are highly thankful to the Gayatri Vidya Parishad College of Engineering (A), Visakhapatnam for providing partial financial support. Ramadevi also thankful to Prof. Dr. Leela Pradhan, Amrit Science Campus, Tribhuvan University and the Kailali Multiple Campus, Farwest University, Dhangadhi, Kailali, for extending the Laboratory facilities.

**References**

[1] E. Fred et al. Solid-state light sources getting smart. *Science*, 308(5726):1274–1278, 2003.

[2] S. Dadgar et al. Optical spectroscopic sensing of tumor hypoxia. *Journal of Biomedical Optics*, 23(6):067001–067001, 2018.

[3] J. Ma et al. Advanced techniques for hyperspectral imaging in the food industry: principles and recent applications. *Annual Review of Food Science and Technology*, 10:197–220, 2019.

[4] L. Zhou et al. Spectral properties and energy transfer of a potential solar energy converter. *Chemistry of Materials*, 28(10):2834–2843, 2016.

[5] G. Hong et al. Near-infrared fluorophores for biomedical imaging. *Nature Biomedical Engineering*, 1(1):0010, 2017.

[6] K. Chrzanowski et al. Review of night vision technology. *Opto-Electronics Review*, 21(2):153–181, 2013.

[7] T. Pulli et al. Advantages of white led lamps and new detector technology in photometry. *Light: Science Applications*, 4(8):e332–e332, 2015.

[8] R. Filippo et al. Leds: sources and intrinsically bandwidth-limited detectors. *Sensors*, 17(7):1673–1684, 2017.

[9] L. Zhang et al. A high efficiency broadband near-infrared $Ca_2LuZr_2Al_3O_{12}$:$Cr^{3+}$ garnet phosphor for blue LED chips. *Journal of Material Chemistry C*, 6(18):4967–4976, 2018.

[10] P.F. Pereira et al. Red, green, and blue (RGB) emission doped $Y_3Al_5O_{12}$ (YAG) phosphors prepared by non-hydrolytic sol-gel route. *Journal of Luminescence*, 130:488–493, 2010.

[11] C. Liu et al. Synthesis, crystal structure, and enhanced luminescence of garnet type $Ca_3Ga_2Ge_3O_{12}$:$Cr^{3+}$ by codoping $Bi^{3+}$. *Journal of American Ceramic Society*, 98(6):1870–1876, 2015.

[12] S.D. Jackson. Efficient $Tm^{3+}$, $Ho^{3+}$-co-doped silica fibre laser diode pumped at 1150 nm. *Optics communications*, 281(18):3837–3840, 2008.

[13] N. Liu et al. Bright white up-conversion emission from $Yb^{3+}/Tm^{3+}/Ho^{3+}$ tri-doped M-$AgGd(WO_4)_2$ phosphors. *Journal of Luminescence*, 152:182–187, 2014.

[14] R. Praveena et al. Photoluminescence properties of $Ho^{3+}/Tm^{3+}$-doped YAGG nanocrystalline powders. *Optical Materials*, 72:666–672, 2017.

[15] Y. Li et al. Long persistent and photostimulated luminescence in $Cr^{3+}$-doped Zn–Ga–Sn–O phosphors for deep and reproducible tissue imaging. *Journal of Material Chemistry C*, 2(15):2657–2663, 2014.

[16] Z. Pan et al. Sunlight-activated long-persistent luminescence in the near-infrared from $Cr^{3+}$-doped zinc gallogermanates. *Naturematerials*, 11(1):58–63, 2012.

[17] B. Qiao et al. Study on $ZnGa_2O_4$:$Cr^{3+}$ ac powder electroluminescent device. *Materials Letters*, 61(2):401–404, 2007.

[18] V. Lupei. $RE^{3+}$ emission in garnets: multisites, energy transfer and quantum efficiency. *Optical Materials*, 19(1):95–107, 2002.

[19] P.F. Pereira et al. Red, green and blue (RGB) emission doped $Y_3Al_5O_{12}$ (YAG) phosphors prepared by non-hydrolytic sol–gel route. *Journal of Luminescence*, 130:488–493, 210.

[20] T.H. Allik et al. Crystallography, spectroscopic analysis, and lasing properties of $Nd^{3+}$:$Y_3Sc_2Al_3O_{12}$. *Physical Review B*, 41(1):21–30, 1990.

[21] L.H. Spangler et al. A computational study of host effects on $Er^{3+}$ upconversion and self quenching efficiency in ten garnets. *Journal of Applied Physics*, 79(10):573–577, 1996.

[22] R. Praveena et al. White light generation from $Dy^{3+}$-doped yttrium aluminium gallium mixed garnet nano-powders. *Journal of Luminescence*, 170:262–270, 2016.

[23] R. Kasuya et al. Glycothermal synthesis and photoluminescence of YAG: $Ce^{3+}$ nanophosphors. *Journal of Alloys and Compounds*, 408(1-2):820–823, 2006.

[24] K. Papagelis et al. Lattice dynamical properties of the rare earth aluminum garnets ($RE_3Al_5O_{12}$). *Physica Status Solidi (b)*, 233(1):134–150, 2002.

[25] K. Papagelis and S. Ves. Vibrational properties of the rare earth aluminum garnets. *Journal of Applied Physics*, 94(11):6491, 2003.

[26] I. Hernandez et al. Inorganic chemistry. *Inorganic Chemistry*, 47:10288–10298, 2008.

[27] M.N. Sanz-Ortiz et al. Origin of the $2E \Longleftrightarrow {}^4T_2$ fano resonance in $Cr^{3+}$-doped $LiCaAlF_6$: Pressure-induced excited-state crossover. *Physical Review B*, 81(4):045114, 2010.

[28] J. Zhou et al. Synthesis and near-infrared luminescence of $La_3GaGe_5O_{16}$:$Cr^{3+}$ phosphors. *RSC Advances*, 4(86):46313–46318, 2014.

[29] Z. Jia et al. Strategies to approach high performance in $Cr^{3+}$-doped phosphors for high-power NIR-LED light sources. *Light: Science Applications*, 9:86, 2020.

[30] H. Yu et al. Broadband near-infrared emission of $K_3ScF_6$:$Cr^{3+}$ phosphors for night vision imaging system sources. *Chemical Engineering Journal*, 417:129271, 2021.

[31] Z. Jia et al. Structural and photoluminescence properties of $Cr^{3+}$doped $LaVo_4$ phosphor. *Light: Science Applications*, 129(9):106904–106915, 2022.

[32] L. Yao et al. Broadband emission of single-phase $Ca_3Sc_2Si_3O_{12}$:$Cr^{3+}$/$Ln^{3+}$ (lLn= Nd, yb, ce) phosphors for novel solid-state light sources with visible to near-infrared light output. *Ceramics International*, 45:14249–14255, 2019.

[33] D. Chen et al. $Yb^{3+}$/$Ln^{3+}$/$Cr^{3+}$ (Ln = Er, Ho) doped transparent glass ceramics: crystallization, $ln^{3+}$ sensitized $Cr^{3+}$ upconversion emission and multi-modal temperature sensing. *Journal of Material Chemistry C*, 5:11769–11780, 2017.

[34] Y. Zhang et al. Enhanced photoluminescence of $Gd_3Al_4GaO_{12}$:$Cr^{3+}$ by energy transfers from Co-doped $Dy^{3+}$ *Nanomaterials*, 12:4183, 2022.

[35] C. Zhong et al. High output power and high quantum efficiency in novel nir phosphor $MgAlGa_{0.7}B_{0.3}O_4$:$Cr^{3+}$ with profound FWHM variation. *Advanced Materials*, 36(10):2309500, 2023.

[36] M. Yamaga et al. Temperature dependence of the lifetime of $Cr^{3+}$ luminescence in garnet crystals i. *Applied Physics B*, 50(4):425–431, 1990.

[37] J. Li et al. Growth, spectroscopic properties, and energy levels of $Cr^{3+}$ doped $LuScO_3$ crystal. *Optical Material Express*, 12(8):3071–3080, 2022.

[38] Y. Guo et al. A red-emitting perovskite-type $SrLa_{(1x)}MgTaO_6$:x$Eu^{3+}$ for white LED application. *Journal of Luminescence*, 167:381–385, 2015.

[39] L. Wu et al. Luminescence and energy transfer of a color tunable phosphor: $Dy^{3+}$-, $Tm^{3+}$-, and $Eu^{3+}$-coactivated $KSr_4(BO_3)_3$ for warm white UV LEDs. *Journal of Materials Chemistry*, 22:6463–6470, 2012.

[40] J. Xiang et al. Enhancement of red emission and site analysis in $Eu^{2+}$ doped new-type structure $Ba_3CaK(PO_4)_3$ for plant growth white LEDs. *Chemical Engineering Journal*, 356:236–244, 2019.

[41] Q. Sun et al. Synthesis and photoluminescence properties of deep red-emitting $CaGdAlO_4$:$Mn^{4+}$ phosphors for plant growth LEDs. *Journal of Luminescence*, 203:371–375, 2018.